PROCEEDINGS OF SCIENCE

Cosmic Ray transport in subAlfvénic magnetohydrodynamic turbulence

A.Marcowith*
Laboratoire Univers et Particules et Montpellier, université de Montpellier, CNRS, France
E-mail: Alexandre.Marcowith@umontpellier.fr

R.Cohet
Laboratoire Univers et Particules et Montpellier, université de Montpellier, CNRS, France
E-mail: Romain.Cohet@umontpellier.fr

Cosmic-Ray mean free paths in magnetized sub-Alfvénic turbulence are calculated using direct numerical simulations coupling kinetic and magnetohydrodynamic (MHD) calculations.The mean free paths are reconstructed by averaging over a large number of particle trajectories and several magnetic realizations. Our solutions depend on the geometry of the turbulence forcing: either compressible or solenoidal. Our results in the compressible forcing case are found to be compatible with the predictions of the quasi-linear theory (QLT), whereas solenoidal forcing solutions are not. This underlines the influences of the different MHD modes over the particle scattering process.

The 34th International Cosmic Ray Conference,
30 July- 6 August, 2015
The Hague, The Netherlands

*Speaker.

PoS(ICRC2015)481

1. Introduction

Cosmic rays (CRs) propagate in our Galaxy through the interaction with electromagnetic perturbations usually described by the magneto-hydrodynamic (MHD) approximation [2] i.e., long wavelength perturbations with scales comparable to the particle's Larmor radius $R_L = v\gamma/\Omega_c$, where $\Omega_c = ZeB/mc$ is the cyclotron pulsation of a particle of mass m and charge Z in a magnetic field of strength B. The detailed modeling of the particle transport in MHD turbulence is complex and request approximations to obtain solutions describing particle trajectories. Transport studies have been first based on the quasi-linear theory (QLT) [1, 2] where the unperturbed (gyro motion) particle trajectory is retained and injected in the electro-magnetic correlation tensor used to derive random Lorentz forces exerted over the particles. QLT is applicable over restricted timescales, intermediate between the pitch-angle particle scattering time and the particle pitch-angle isotropization time. The main drawback of QLT is that it produces pathological particle parallel mean free paths because of infinite values of the cosine pitch-angle diffusion coefficient at 90 degrees. Several analytical approaches have been proposed to cure this issue [3]. In particular the 90 degree scattering problem has been proposed to be solved by the mean of the broadening of the resonance [4]. However, the way the resonance has to be broaden and the non-linear solutions which have to be retained into diffusion coefficient calculations are dependent on the model of the background turbulence. Needless to say that all these studies are performed in the test-particle approximation (see [5]). It is known that when the density in the relativistic particles is high enough the particles can generated their own waves and induce a modification of the turbulence [6, 7].
Another difficulty of the CR transport resides in the description of MHD turbulence, hence in the mathematical description of the random Lorentz forces. In the incompressible limit, MHD turbulence is described by an anisotropic model [8, 9]. In this model, due to Alfvenic turbulence dynamics the perturbations are elongated along the magnetic field and follow the scaling $k_\parallel \ell^{1/3} = k_\perp^{2/3}$ (Goldreich-Sridhar scaling or GS scaling hereafter). This relation is due to a critical balance between $(k_\perp v_\perp)^{-1}$ the perpendicular cascade time and $(k_\parallel v_a)^{-1}$ the Alfvén wave packets crossing time. Hereafter the following notations are adopted: here $k_{\parallel/\perp}$ have to be understood as the parallel/perpendicular component of the wave number with respect to the local magnetic field, $v_\perp$ is the perpendicular perturbations velocity and v_a is the local Alfvén velocity. The local magnetic field is not unique, its direction in fact depends on the scale $1/k_\parallel$ under consideration as explained in [10]. In the compressible limit, using direct numerical MHD simulations (DNS), [11] confirmed that Alfvénic turbulence follows a GS spectrum and show that fast-magnetosonic turbulence follows an isotropic Kraichnan spectrum.
In this work we perform DNS MHD simulations and couple them to the Lorentz force by upgrading the `RAMSES` MHD code [12, 13] with a turbulence forcing module (see §2.1) and a kinetic module (see §2.2). We present particle mean free paths calculation in §3.

2. Code description

2.1 Magneto-hydrodynamic simulations

The MHD simulations performed in this work have been obtained in a 3D cartesian geometry with periodical boundary conditions. The simulation box has a size $L = 1$ which can be rescaled

afterward to fit the problem under consideration. The turbulence is generated by forcing the fluid velocity component with an external force $\vec{f}$ in both Euler and energy equations. The force is expressed in terms of its Fourier transform $\hat{f}$ and enters into a stochastic Ornstein-Uhlenbeck process. A detailed description of the implementation of the forcing is described in [14] but we reproduce it for completion here. The components of the force are expressed in terms of the Fourier amplitudes of N_m modes:

$$f_i = \Sigma_m \hat{f}_{i,m} \cos(2\pi k_{j,m} x_j) \ , \tag{2.1}$$

where $\hat{f}_{i,m}$ are initialized to zero at the beginning of each MHD run. Each mode follows a stochastic differential equation

$$d\hat{f}_{i,m} = g_\chi \times \left[-\bar{\varepsilon} \hat{f}_{i,m} \frac{dt}{T} + \bar{\beta} \frac{V}{T} \sqrt{\frac{2w(k)^2}{T}} P^\chi_{i,j,m} d\xi_j \right] \ . \tag{2.2}$$

The different parameters entering in the forcing are: w the amplitude of the forcing, T the auto-correlation time scale, $\bar{\varepsilon}$, $\bar{\beta}$ are parameters controlling the relative strength of the decay and driven forcing components ($\bar{\varepsilon} = \bar{\beta} = 1$ has been adopted in this work), $d\xi_j = \xi_j \sqrt{dt}$. The random variable ξ_j is sampled over a Gaussian distribution of zero mean and variance one. $P^\chi_{i,j,m}$ is a tensor that defines the geometry of the forcing [15]

$$P^\chi_{i,j,m} = \chi \delta_{i,j} + (1 - 2\chi) \frac{k_i k_j}{k^2} \ . \tag{2.3}$$

$\chi \in [0,1]$ controls the relative importance of solenoidal and compressive modes in the random forcing operator entering in the Ornstein-Uhlenbeck process. Hence, $\chi = 0$ corresponds to a pure compressive forcing (CF) and $\chi = 1$ corresponds to a pure solenoidal forcing (SF). The normalization factor $g_\chi = 3/\sqrt{1 - 2\chi + 3\chi^2}$.

In all simulations the isothermal approximation for the gas equation of state has been used. The simulation set up are $P = \rho = 1$ and a sound speed is $c_{s0} = \sqrt{\gamma} \simeq 1.005$ and $V = c_s$. The energy is injected into large scale modes in the wavenumber interval $k \in]1,3] \times 2\pi/N$ (w is an Heaviside function), where N is defined by the level of refinement X as $N = 2^X$. Notice that hereafter we make the distinction between L the size of simulation cube and $L_{inj} < L$ the scale of turbulence injection identified with the coherence length of the turbulence. Typically we have $L_{inj} \sim 0.1 - 0.2L$

We performed different type of MHD simulations: with different levels of refinement L=8, 9 or 10, the intensity of the turbulence characterized by $\langle M_s \rangle$ and $\langle M_a \rangle$ the mean sonic and Alfvénic Mach numbers, is controlled by the parameter w. The mean sonic and Alfvénic Mach numbers are obtained after the turbulent spectrum has reached a quasi-stationary state and averaging over three snapshots that will be used as turbulent field realizations for the propagation of the particles. Each snapshot are separated by at least 2 cascading time scales at large scales (i.e. 2 L/V, V is the perturbation velocity). The MHD simulations have been performed at the CINES center on the Jade and Occigen super calculators. The typical duration of a MHD run at 256^3, 512^3 and 1024^3 are 5000, 20000 and 90000 h.cpu.

2.2 The kinetic module

We solved the Lorentz equation for each particle of charge q and mass m. Particles have a momentum $\vec{p} = \gamma m \vec{v}$ and a normalized velocity $\vec{\beta} = \vec{v}/c$ and propagate in an electromagnetic field $\delta\vec{E}$ (no mean electric field), $\vec{B}_T = \delta\vec{B} + \vec{B}_0$:

$$\begin{aligned} \frac{d\vec{p}}{dt} &= q\delta\vec{E} + q\vec{\beta} \wedge \vec{B}_T \ , \\ \frac{d\vec{r}}{dt} &= \vec{v} \ . \end{aligned} \tag{2.4}$$

The electromagnetic fluctuating components $\delta\vec{E}, \delta\vec{B}$ are provided by the MHD code. In this work only protons are considered, hence $m = m_p$ and $q = +e$. Each particle is injected with a Lorentz factor γ_0. This defines the particle's Larmor radius $r_{L0} = \gamma_0 mc^2/eB_0$. We also define the particle's synchrotron pulsation $\Omega_0 = r_{L0}/c$. Eq. 2.4 is normalized with respect to this initial value as (see [16]):

$$\frac{d\hat{u}}{d\hat{t}} = \hat{\gamma}\frac{\delta\vec{E}}{B_0} + \hat{u} \wedge (\frac{\delta\vec{B}}{B_0} + \vec{e}_z) \ , \tag{2.5}$$

$$\frac{d\hat{x}}{d\hat{t}} = \frac{r_{L0}}{L} \wedge \hat{u} \ . \tag{2.6}$$

We have assumed that the large scale magnetic field $\vec{B}_0$ is aligned along $\vec{e}_z$. In the previous equations we have the following notations: $\hat{u} = \hat{\gamma}\vec{\beta}$, $\hat{\gamma} = \gamma/\gamma_0$, $\hat{t} = t \times (\hat{\gamma} r_{L0}/c)^{-1}$. In practice in the ISM the effect of the electric field over high-energy (multi TeV) CRs can be neglected and $\hat{\gamma}$ remains equals to 1 if losses can be neglected.

We have tested several integration schemes to solve Eq. 2.5 and 2.6: a leap-frog scheme (by default implemented in `RAMSES` to treat the propagation of test particles in the gravitational field), a Runge-Kutta method of 5th order and a Bulirsch-Stoer method ([17]). We found differences between the methods at the level of a few percent over the particle mean free paths. The leap-frog integration method has been used in this work to save computational ressources. The typical duration of one run to complete the propagation of 10^6 particles depends on the particle's rigidity and the Alfvénic Mach number. It varies from 10^6 to a few 10^7 time steps, that is 13 to few hundred hours of computing on the supercomputers JADE and OCCIGEN at the CINES facility. The magnetic field is interpolated at the position of the particle from its values derived by the MHD code at the grid points. For this we have adopted a volume averaged interpolation of the field strength. The volume can include the next 8 neighbor points, this is the first order cloud-in-cell (CIC) interpolation implemented by default in `RAMSES` or the next 64 neighbor points using a third order piecewise cubic spline (PCS) interpolation ([18]). The results in this work have been obtained using the PCS interpolation method.

3. Mean free path studies

3.1 CR mean free path: Calculation procedure

The CR mean free path is reconstructed using an averaging procedure over a large number of individual particle trajectories. For each particle we record their position x, y, z in the 3D simula-

tion cube: $z(t)$ determines the position of the particle with respect to the global magnetic field $\vec{B}_0$, $x(t), y(t)$ determines the position of the particle in directions perpendicular to the global magnetic field $\vec{B}_0$.

To proceed to the mean free path calculation, we have selected a set of $N_r = 3$ magnetic field realizations separated by at least 2 large scale cascade time in order to ensure a statistical independence between two successive realizations. For each realization an ensemble of N_p particles are propagated until a convergence is obtained (see next). The parallel spatial diffusion coefficient is calculated using the following formula:

$$\kappa_{\parallel}(t) = \frac{\langle (z(t) - z(0))^2 \rangle}{2t} = \frac{1}{N_r} \frac{1}{N_p} \Sigma_{i=1}^{N_r} \Sigma_{j=1}^{N_p} \frac{(z_{i,j}(t) - z_{i,j}(0))^2}{2t} \ . \tag{3.1}$$

The perpendicular spatial diffusion coefficient is calculated using the following formula:

$$\kappa_{\perp}(t) = \frac{1}{N_r} \frac{1}{N_p} \Sigma_{i=1}^{N_r} \Sigma_{j=1}^{N_p} \frac{(x_{i,j}(t) - x_{i,j}(0))^2 + (y_{i,j}(t) - y_{i,j}(0))^2}{4t} \ . \tag{3.2}$$

The two above coefficients are calculated until they both converge to a plateau. Once the diffusion coefficient $\kappa_{\parallel,\perp} = \lim_{t \to +\infty} \kappa_{\parallel,\perp}(t)$ is found, the corresponding mean free path is obtained through the relation $\lambda_{\parallel,\perp} = 3\kappa_{\parallel,\perp}/v$ (the particle velocity $v = c$). For the results presented below a typical number of $N_p = 10^6$ particles have been used.

3.2 Mean free path-Alfvénic Mach number dependence

Figures 1 and 2 present the dependences of CR parallel and perpendicular mean free paths with respect to the Alfvénic Mach number $M_a \sim V/V_a$ (where V is the level of perturbations of the velocity field) .

We first compare our results in the SF case with the results of [19] (XY13 hereafter). XY13 performed level=9 simulations using an incompressible forcing but with another MHD code. The mean free paths have been calculated at normalized rigidities $\rho = r_L/L = 0.01$. Hence, comparing our figure 1 (upper figure, red points) with figure 5 in XY13 we clearly see disagreements especially in the regime $M_a < 0.7$ where we find $\lambda_{\parallel}/L > 100$ whereas XY13 find mean free paths $\lambda_{\parallel}/L < 10$. At higher Alfvénic Mach numbers although the results are compatible. Turning now to perpendicular mean free paths (the red points in our upper figure 2 and figure 6 in XY13) we find a reasonably good agreement: our index $\alpha = 2.94 \pm 0.69$ is compatible with the index found by XY13 $\alpha = 4.21 \pm 0.75$. The normalization of the mean free paths are also compatible since we normalize $\lambda_{\perp}$ to the box length L whereas XY13 did normalized $\lambda_{\perp}$ to the injection scale of the turbulence L_{inj}. We can advance different reasons to explain the discrepancies between the two calculations. First, even if the forcing is in both cases incompressible, the forcing method is not likely similar in the two MHD codes. Then, the structure and the methods used in the two MHD codes to derive the fluid solutions are likely different. Finally, XY13 derive their solutions at $\rho = 0.01$. Particles at these energies do have a Larmor radius that is in resonance with perturbations that are in the dissipation range of the turbulence for simulations at 512^3 resolution. This effect is particularly important for the scattering of particles parallel to the magnetic field. This is the main reason why concerning the problem of propagation of CR in MHD turbulence the results derived at $\rho = 0.01$

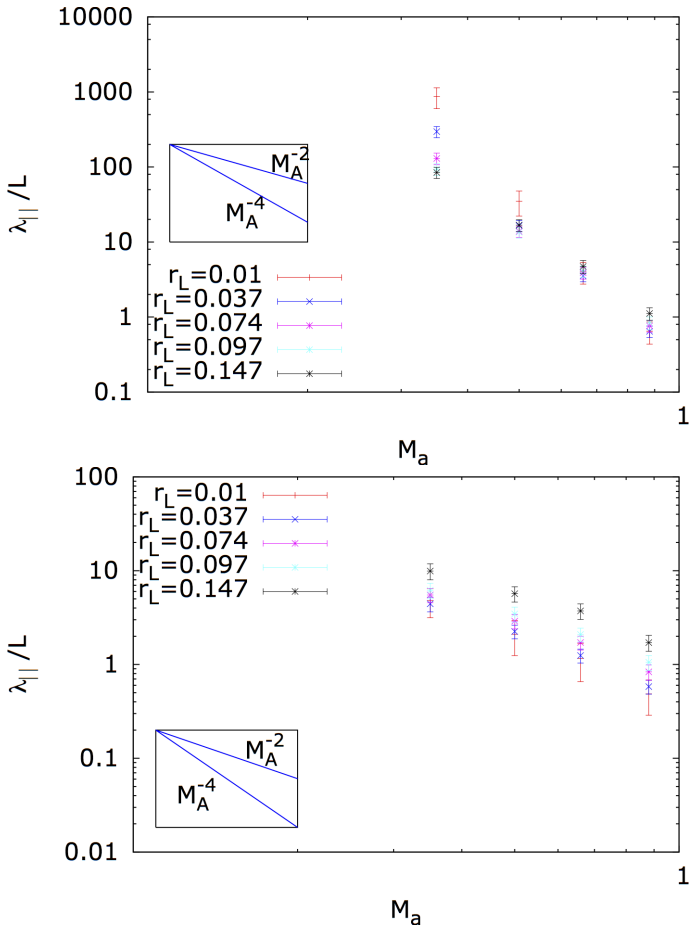

Figure 1: Upper figure: parallel mean free path versus Alfvénic Mach numbers M_a at different particle rigidities in the SF case. Lower figure: parallel mean free path versus Alfvénic Mach numbers M_a at different particle rigidities in the CF case. M_a^{-2} and M_a^{-4} dependences have been also inserted.

have to be interpreted with some care. Next, the results are discussed for particles with $\rho > 0.01$.

We find parallel mean paths compatible with M_a^{-2} in the CF case. The SF case shows steeper dependencies compatible with M_a^{-4}. It is clear comparing upper and lower figures in Fig.1 that SF produces a turbulent spectrum that is much less efficient at scattering particles. The SF forcing is expected to favor the production of Alfvén modes with respect to fast- and slow-magnetosonic modes. Recent transport models (see eg [10]) concluded that Alfvénic turbulence scatters CRs rather inefficiently because of the strong anisotropy the perturbations developed towards the smallest scales. Here, we found typical ratios $\lambda_{\|}(\chi = 1)/\lambda_{\|}(\chi = 0) < 100$ which are not as small as predicted by these analytical models. This is likely because both compressible and incompressible modes are produced in the two forcing geometries [11]. Any more quantitative discussion would require to isolate the effects of each mode that composes the turbulent spectrum in the different forcing limits.

Concerning perpendicular mean free paths, we can compare our results with the theoretical predictions proposed in [7] in the regime of sub-Alfvénic turbulence. If $\lambda_{\|}/L_{inj} > 1$ then [7] predict

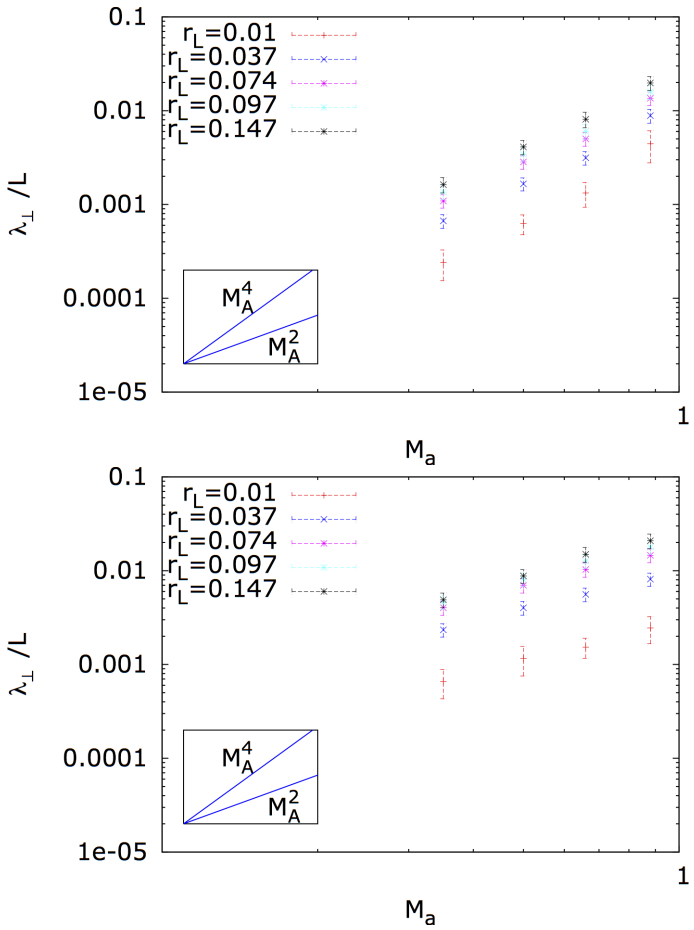

Figure 2: Upper figure: perpendicular mean free path versus Alfvénic Mach numbers M_a at different particle rigidities in the SF case. Lower figure: perpendicular mean free path versus Alfvénic Mach numbers M_a at different particle rigidities in the CF case.

$\lambda_\perp/L_{inj} = 1/3M_a^4$, and if $\lambda_\parallel/L_{inj} < 1$ then $\lambda_\perp = \lambda_\parallel M_a^4$. In the SF case we have $\lambda_\parallel/L_{inj}$ which scans the range $1-10^3$. We find $\lambda_\perp \propto M_a^{2.52\pm0.26}$ for a particle at $\rho = 0.097$, so not compatible (but close) with the above theoretical limit of $\lambda_\perp \propto M_a^4$. Notice however that at high M_a we have $\lambda_\parallel/L_{inj} \geq 1$, but not $\gg 1$, this may explain the difference. The extrapolation of $\lambda_\perp$ (accounting for the error over the index) at high M_a produces $\lambda_\perp/L_{inj}(\rho = 0.097) \sim 1/3$. In the CF case, our solution is $\lambda_\perp \propto M_a^{1.42\pm0.37}$. As $\lambda_\parallel$ is reduced with respect to the SF case we have tested the relation $\lambda_\perp = \lambda_\parallel M_a^4$. We found that our result is not compatible with the latter relation and it is also strongly incompatible with $\lambda_\perp \propto M_a^4$. Here again, the parallel mean free paths cover a range $(1-50)L_{inj}$. This may explain that we do not find a clear trend. In both forcing geometries our solutions are relatively close to $\lambda_\perp \propto M_a^2$ corresponding to the field line wandering (FLW) limit (see [1]) obtained within the framework of QLT.

4. Conclusion

In summary, our results are globally consistent with the results provided by XY13 to the notable exception of $\lambda_\parallel$ at $M_a < 0.7$. This effect is may be connected with differences in the forcing

procedures and methods used to solve the MHD equations in the two codes. But we consider that the results at low rigidity have to be considered with some caution because there particles are in resonance with perturbations which are in the turbulent dissipation range. Concerning particles with higher rigidities we have the following results: compressible forcing produces more efficient particle scattering and smaller parallel mean free paths which can be two orders of magnitude smaller than what is found for an solenoidal forcing. CF results are compatible with QLT predictions. This result is consistent with the fact the magnetosonic waves are preferentially produced in the CF geometry whereas shear Alfvén waves are preferentially produces in the SF geometry. Our results concerning $\lambda_\perp$ have not been found to be fully compatible with the theoretical predictions proposed in [7]. This may be explained that for each χ values the parallel mean free path is not entirely in the regime $\lambda_\parallel/L_{inj} \gg 1$ or $\lambda_\parallel/L_{inj} \ll 1$. Our solutions are not fully compatible but close to the FLW M_a^2 scaling. More extensive calculations with higher resolutions to get ride of forcing effects are required to obtained definite conclusions.

References

[1] Jokipii J.R., 1966, ApJ, 146, 480.

[2] Schlickeiser R., 2002, Cosmic Rays Astrophysics, Springer.

[3] Shalchi A., 2009, Astrophysics and Space Science Library, Vol. 362, Non- linear Cosmic Ray Diffusion Theories.

[4] Völk, H. J. 1973, ApSS, 25, 471

[5] Ptuskin, V. S., et al. 2006, ApJ, 642, 902.

[6] Farmer, A. J. Goldreich, P. 2004, ApJ, 604, 671.

[7] Yan, H. Lazarian, A. 2008, ApJ, 673, 942.

[8] Goldreich, P. Sridhar, S. 1995, ApJ, 438, 763.

[9] Maron, J. Goldreich, P. 2001, ApJ, 554, 1175.

[10] Chandran, B. D. G. 2000, Physical Review Letters, 85, 4656

[11] Cho, J. Lazarian, A. 2003, MNRAS, 345, 325.

[12] Teyssier, R. 2002, AA, 385, 337.

[13] Fromang, S., Hennebelle, P., Teyssier, R. 2006, AA, 457, 371.

[14] Schmidt, W., et al. 2009, AA, 494, 127.

[15] Federrath, C., Klessen, R. S., Schmidt, W. 2008, ApJ, 688, L79.

[16] Beresnyak, A., Yan, H., Lazarian, A. 2011, ApJ, 728, 60.

[17] Press, W. H., Teukolsky, S. A., Vetterling, W. T., Flannery, B. P. 1992, Numer- ical recipes in FORTRAN. The art of scientific computing.

[18] Haugboelle, T., Frederiksen, J. T., Nordlund, A. . 2013, Physics of Plasmas, 20, 062904.

[19] Xu, S. Yan, H. 2013, ApJ, 779, 140.